JOURNAL OF APPLIED ELECTROCHEMISTRY 25 (1995) 667–670

Electrodeposition of Ni–Mo alloys with pulse reverse potentials

E. CHASSAING, M. P. ROUMEGAS, M. F. TRICHET

Centre d'Etudes de Chimie Métallurgique, CNRS, 15 rue Georges Urbain, 94407 Vitry-sur-Seine, France

Received 28 November 1994; revised 8 January 1995

With the aim of improving the protective properties of Ni–Mo alloy layers, pulse reverse electrodeposition has been investigated. The anodic pulses were applied in the potential range where hydrogen desorption and oxidation occur. The alloy composition was shown to depend on the pulse parameters, especially on the anodic pulse duration. For long anodic pulses a preferential dissolution of molybdenum in the electrodeposited alloy occurs, while bulk Ni–Mo alloys do not undergo any dissolution. For anodic pulses longer than a certain threshold the electrocrystallization process becomes blocked. The morphology and microstructure of the layers are mainly determined by the molybdenum content rather than by the pulse parameters.

1. Introduction

Due to the high corrosion resistance of Ni–Mo alloys in several aggressive environments, the electrodeposition of these alloys has received much attention [1–10]. Though molybdenum cannot be separately deposited in aqueous solutions its codischarge may be 'induced' by the presence of an iron-group metal such as Fe, Co or Ni [1]. An electrocrystallization mechanism has been developed [8] and deposition conditions have been found in direct and in pulse plating which allow the preparation of protective coatings containing about 20 wt % molybdenum [3, 9]. However, layers with large molybdenum content have a tendency to crack due to high internal stresses. These stresses may be connected with the hydrogen evolution process.

Recently a voltammetric investigation of Ni–Mo electrolytes has emphasized the role of hydrogen in the electrocrystallization of these alloys and showed that, during the anodic scan, a peak attributed to the oxidation of hydrogen appears [11].

The present work is aimed at investigating the properties of Ni–Mo layers pulse-plated with anodic pulses in the potential range where anodic oxidation of hydrogen occurs. Several investigations have pointed out the beneficial effects of pulse reverse plating. Anodic pulses may have a levelling influence leading to increased brightness and improved mechanical properties as a result of reduced hydrogen content [12–15].

2. Experimental procedure

A double-wall cell (250 ml) thermostatted at 25 °C was used. The electrolytes, made up of reagent grade chemicals, were deaerated by nitrogen bubbling. The electrolyte composition was chosen from previous investigations: it contained 0.2 M $NiSO_4.7H_2O$, 0.25 M sodium citrate ($Na_3C_6H_5O_7.2H_2O$). The pH was adjusted to 9 by ammonia. A relatively large molybdate concentration (0.06 M $Na_2MoO_4.2H_2O$) was chosen to emphasize the effect of molybdenum and hydrogen evolution on the electrodeposition process, since it is known that the faradaic efficiency markedly decreases when the molybdate concentration is large [1].

A saturated calomel electrode was used as a reference. The auxiliary electrode was a large area nickel sheet. Various working electrodes were used for the voltammetric investigation: nickel, mild steel, platinum, glassy carbon discs. For the d.c. and pulse reverse experiments the Ni–Mo layers were deposited on mild steel plates (4 cm^2) polished, degreased and etched prior to each experiment. For comparison a synthetic Ni–Mo alloy (19 wt % Mo) was prepared by induction plasma melting from high-purity nickel and molybdenum (Johnson–Matthey less than 10 ppm impurities). Voltammetric investigation and pulse plating experiments were carried out, under potentiostatic control, by means of a Schlumberger 1186 electrochemical interface monitored by a microcomputer using homemade softwares.

The Ni–Mo layers were examined by scanning electron microscopy (SEM) using secondary electron emission and analysed by energy dispersive X-ray spectroscopy (EDX). The faradaic efficiency of the deposition process was calculated from the mass increase and the electrical charge used taking into account the chemical composition of the deposits. Their structure was characterized by X-ray diffraction (cobalt anticathode, $\lambda_{K\alpha} = 178.89$ pm).

3. Preliminary investigations

Cyclic voltammograms have been recorded at 50 mV s^{-1} with various substrates (Fig. 1). The voltammograms are similar to those obtained by

0021-891X

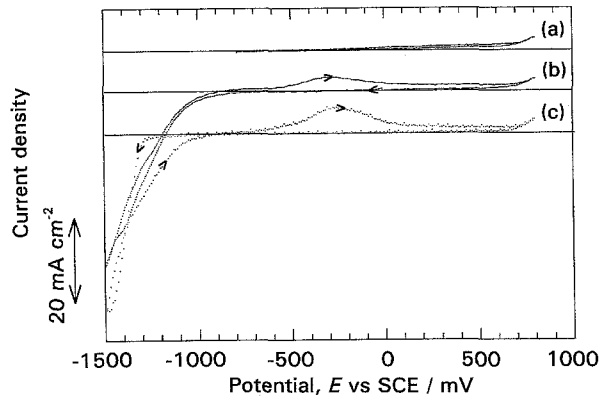

Fig. 1. Cyclic voltammogram recorded at 50 mV s^{-1}. (a) Ni–Mo massive alloy from +800 to −800 mV vs SCE, (b) Ni–Mo massive alloy from +800 to −1500 mV vs SCE, (c) glassy carbon electrode from +800, to −1500 mV vs SCE.

Crousier *et al.* [11]. Whatever the substrate nature, even with the Ni–Mo massive alloy, the current is negligible for voltammograms recorded between −1000 and +800 mV (Fig. 1, curve (a)): hence no dissolution reaction of the Ni–Mo alloys occurs in this potential range. When the cathodic limit is shifted towards more negative potentials, the Ni–Mo discharge is observed on the forward scan (Fig. 1, curves (b) and (c)). On the reverse scan, whatever the nature of the substrate, a broad anodic peak occurs at $E = -250$ mV. It is more pronounced with the glassy carbon electrode (curve (c)) than with metallic ones (curve (b)), in which hydrogen may penetrate. The anodic charge used for this reaction is much lower than the cathodic one. In agreement with Crousier *et al.* [11], we conclude that the anodic peak is not related to a dissolution reaction of the deposit but to the oxidation of the codischarged hydrogen weakly trapped in the layer.

The properties of the layers deposited under d.c. conditions were investigated. At low polarization (Fig. 2) partial current densities for Ni and Mo discharge are nearly equal, leading to Ni–Mo alloys of constant metallic content (stoichiometry close to Ni_3Mo, i.e. 35 wt % Mo) as already observed for electrolytes with a lower molybdate concentration [8]. With increasing polarization, the molybdenum

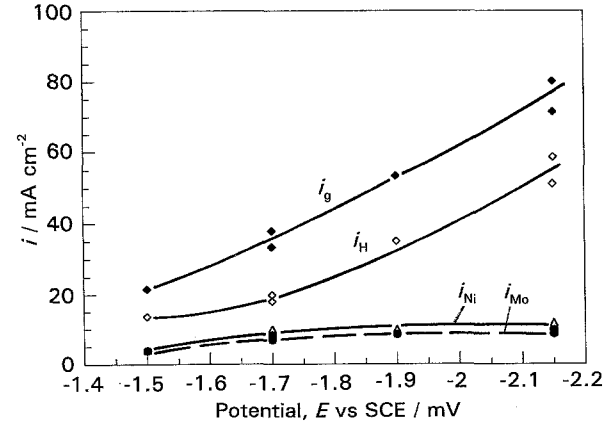

Fig. 2. Global and partial steady-state polarization curves. (i_g) Global polarization curve; (i_H) partial curve for hydrogen evolution; (i_{Ni}) partial curve for nickel discharge; (i_{Mo}) partial curve for molybdenum discharge.

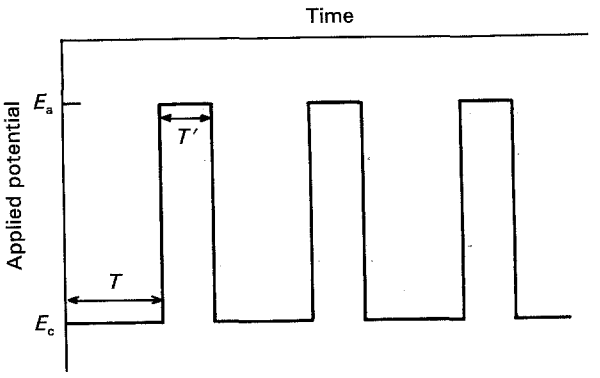

Fig. 3. Scheme of the potential pulses. E_c, cathodic pulse potential; E_a, anodic potential; T, cathodic pulse time; T', anodic pulse time.

content decreases slightly. Over the whole polarization range, hydrogen evolution is the predominant reaction. The faradaic efficiency is rather low and exhibits a maximum at about 45% for a deposition potential of −1700 mV.

4. Pulse reverse deposition

4.1. *Effect of pulse parameters on composition and current efficiency*

Rectangular pulses were applied as shown in Fig. 3. The values of the cathodic potential, E_c, and the anodic potential, E_a, were chosen from the d.c. and voltammetric investigations.

E_c was varied from −2.0 to −3.0 V. As expected from d.c. results, the molybdenum content in the deposit decreases with increasing the cathodic polarization. For large polarization, the layer morphology becomes very irregular and many pits occur. For the following experiments, a deposition potential of −2150 mV was chosen to minimize pitting. Two anodic potentials, E_a, were investigated: −250 and −100 mV, that is, in the range of the anodic peak observed on the voltammograms. The pulse times, T and T', were varied between 10 and 200 ms.

Figure 4 shows the layer composition as a function of the various parameters. When the pulse time, T, is

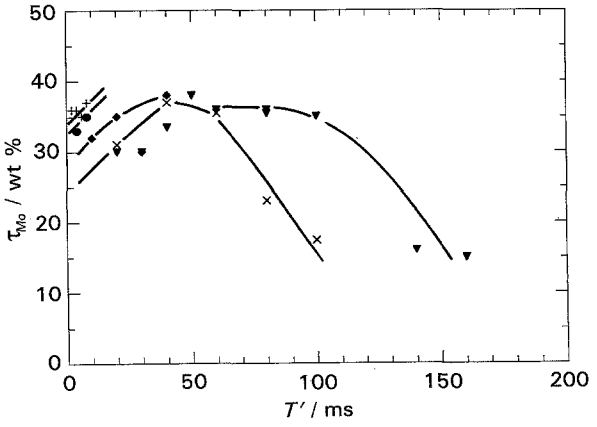

Fig. 4. Molybdenum content in the deposit as a function of the anodic pulse duration, T' for $E_c = -2150$ mV vs SCE and E_a/mV vs SCE: (a, +) −250 for $T = 10$ ms; (b, ●) −250 for $T = 20$ ms; (c, ◆) −250 for $T = 50$ ms; (d, ▼) −250 for $T = 100$ ms; and (e, ×) −100 for $T = 100$ ms.

Table 1. Anodic pulse threshold, T'_0, values for various anodic potential pulses and cathodic pulse durations

E_a/mV vs SCE	T/ms	T'_0/ms
−100	100	100
−250	100	160
−250	10	8

increased (curves (a) to (d)), the molybdenum content, τ_{Mo}, decreases, thus indicating that the deposit composition is partly controlled by diffusion of the Mo(VI) species. The molybdenum content is larger than in d.c. deposited layers at this potential for which τ_{Mo} equal to 29 wt % was measured.

The influence of the anodic pulse duration, T', on the molybdenum content shows three different domains (curves (d) and (e)). For anodic pulse durations up to 50 ms, the molybdenum content increases with T' as a result of Mo(VI) interfacial replenishment, whatever the anodic potential (−100 or −250 mV). For intermediate values of T', the molybdenum content is nearly constant. Such behaviour was already observed in 'normal' pulse plating with relaxation periods at open circuit [9]. For larger T' values, which depend on the anodic pulse potential, the molybdenum content steeply decreases. Above a certain threshold, T'_0, no deposit occurs. This threshold T'_0 increases with the cathodic pulse duration and is larger when the anodic pulse potential, E_a, is more negative (Table 1). Hence, the processes occurring during the anodic pulses are more complicated than metal species replenishment and hydrogen oxidation.

When the anodic pulse duration is increased the current efficiency first decreases and then tends to a constant value up to the threshold T'_0. The cathodic and anodic charges, Q_c and Q_a, were calculated by integration of the current/time responses. The cathodic charge Q_c is the sum of the charge used for hydrogen evolution, $Q_{c(H)}$, and for the alloy deposition, $Q_{c(Ni-Mo)}$. If the only anodic reaction is the oxidation of hydrogen, then: $Q_a = Q_{a(H)}$. If only a certain fraction, β, of the codischarged hydrogen is reoxidized, then $Q_{a(H)} = \beta \times Q_{c(H)}$. The faradaic

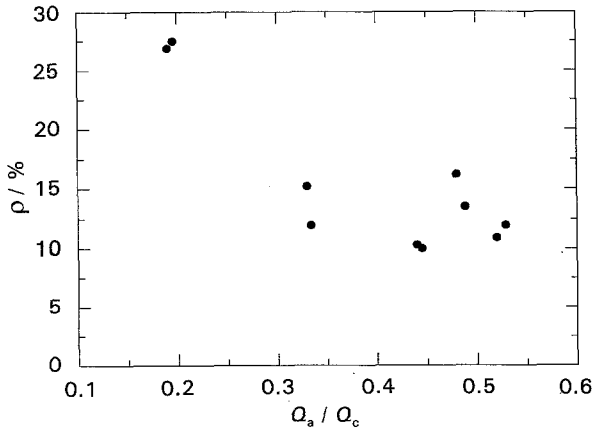

Fig. 5. Cathode current efficiency as a function of the ratio Q_a/Q_c of the anodic and cathodic charges. $E_c = -2150$ mV vs SCE, $E_a = -100$ mV vs SCE, $T = 100$ ms.

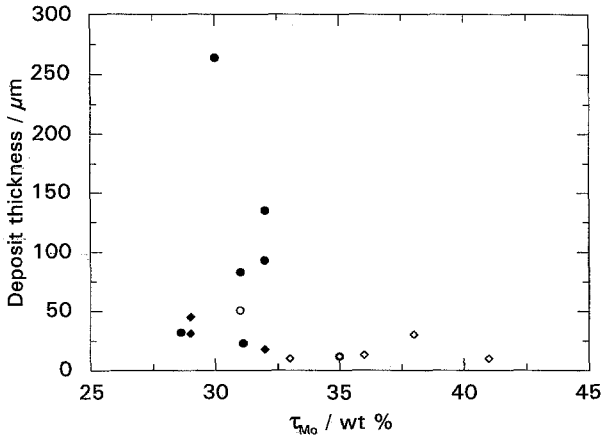

Fig. 6. Crack-free thickness of various Ni–Mo layers as a function of their molybdenum content. Key: (●) d.c., crack-free; (○) d.c., cracked; (◆) p.r., crack-free; (◇) p.r., cracked.

efficiency, ρ, is equal to

$$\rho = \frac{Q_{c(Ni-Mo)}}{Q_c} = 1 - \frac{Q_{c(H)}}{Q_c}$$

where $Q_{c(H)} = Q_{a(H)}/\beta = Q_a/\beta$, then $\rho = 1 - Q_a/\beta Q_c$.

For a given cathodic pulse duration, when the anodic pulse time is increased, the ratio Q_a/Q_c increases, since Q_c is a constant. If hydrogen oxidation is the only electrochemical reaction occurring during the anodic step and if the coefficient β is constant, then the faradaic efficiency should decrease linearly when T' is increased. Such behaviour was observed for palladium deposited under pulse reverse current; a constant β value close to 1 was found [15]. Figure 5 shows that, for large T' values the faradaic efficiency for Ni–Mo deposition does not decrease linearly, indicating that another anodic reaction may occur.

To clarify the effect of the anodic pulse, the current transients were recorded during the various potential pulses. They do not present any appreciable dependence on T', probably because hydrogen evolution is the major cathodic reaction. No difference is observed for times T' longer than the threshold, T'_0, for which the electrocrystallization is blocked, neither in the cathodic nor in the anodic pulses.

4.2. *Discussion*

During the cathodic pulses, metallic species are consumed and hydrogen is codischarged. The depletion is especially marked for the Mo(VI) species whose discharge is partly under diffusion control at these high polarizations [8, 9].

During the anodic pulses, several processes may occur: replenishment of metallic species, hydrogen oxidation and possibly passivation or poisoning of growth sites [14, 16]. As mentioned above the bulk synthetic Ni–Mo alloy does not undergo anodic dissolution in the range −250 to −100 mV, nor does nickel. However, the Ni–Mo deposit, as well as molybdenum, exhibits an anodic current density of about 5 mA cm^{-2} when polarised at −100 mV, indicating a dissolution reaction. Indeed a Ni–Mo layer deposited at a constant potential ($E_p = -2.15$ V,

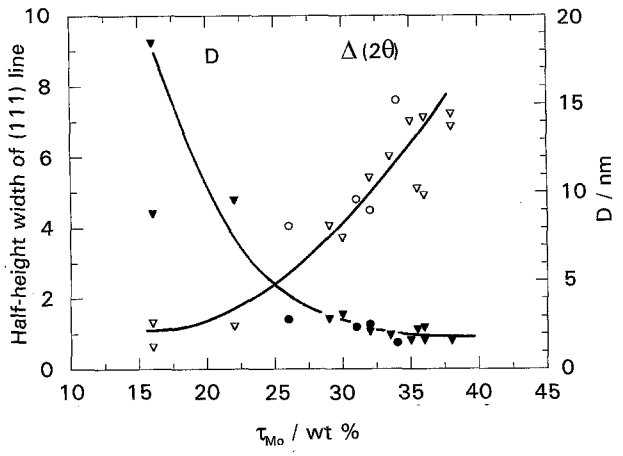

Fig. 7. Half-height width, $\Delta(2\theta)$, of the (1 1 1) XRD peak and crystallite size, D, as a function of molybdenum content. (○) $\Delta(2\theta)$, pulse reverse deposition; (△) $\Delta(2\theta)$, direct current deposition at various potentials; (●) D, pulse reverse deposition; (▲) D, direct current deposition.

containing 29 wt % Mo) was held for 3600 s at −100 mV. EDX analysis shows that the molybdenum content has decreased to 16 wt %, indicating preferential dissolution of molybdenum. The deposit is then much more reactive than the bulk alloy. This feature may be related to the less perfect crystalline structure and to the large amount of incorporated hydrogen. Previous investigations have shown that the corrosion resistance of these layers was markedly improved after a recrystallization heat treatment [3]. This slow preferential anodic dissolution of molybdenum might explain the decrease in the molybdenum content observed for long T' pulse durations.

For anodic pulses longer than a certain threshold, T'_0, the deposition is totally blocked. A complete poisoning of the growth sites due to anion adsorption may have occurred. If these adsorbed species act as hydrogen inhibitors they will block the discharge process, since it has been shown that hydrogen coreduction is necessary for the Ni–Mo codischarge [9–11].

5. Morphology and structure

The Ni–Mo coatings have a nodular morphology. Layers deposited with pulse reverse potentials at relatively large pulse frequencies (i.e., 50–100 Hz) are very bright. The roughness does not increase with deposit thickness. Molybdenum-rich layers often show cracks. Whatever the plating mode (i.e., direct or pulse plating) the crack-free thickness is very low for layers containing more than 30 wt % Mo (Fig. 6).

X-Ray diffraction (XRD) shows that the crystalline state of the layers depends on the pulse parameters. For short anodic pulses, the deposits are mostly amorphous i.e. showing only a broad halo centred on the (1 1 1) peak with a half-height width larger than 6°. For long T' values, the deposits are better crystallized and present a (1 1 1) preferred orientation. Their XRD diagrams present the characteristic lines of the Ni–Mo f.c.c. solid solution. Figure 7 shows that the microcrystalline state is mainly determined by the molybdenum content rather than by the plating mode. The crystallite size calculated from Scherrer's formula varies from about a few nanometres for layers containing more than 30 wt % to 100 nm for alloys containing 15 wt % Mo, whatever the deposition mode, direct or pulse reverse. These results are in agreement with Nee *et al.* who pointed out that the grain size in Ni–Mo deposits is directly related to their composition [10].

When the molybdenum content exceeds 30 wt %, whatever the plating mode, the crack-free thickness and the crystallite size markedly decrease, and the micro and macrostresses increase. This marked transition may be related to the increased supersaturation of the Ni–Mo solid solution.

6. Conclusion

The voltammetric investigation of Ni–Mo electrolytes on various substrates shows that a potential range exists where the oxidation of occluded hydrogen occurs. The electrodeposition of Ni–Mo alloys was carried out under pulse reverse potential in this potential range. Preferential dissolution of molybdenum from the electrodeposited layer may occur whereas massive Ni–Mo alloys do not undergo any dissolution in these solutions. In addition long anodic pulses lead to blocking of the electrocrystallization process.

Layers deposited under pulse reverse potentials show a nodular morphology whose roughness does not increase with thickness by contrast with d.c. deposited layers. However the properties of these coatings mainly depend on the molybdenum content rather on the deposition mode (d.c., pulse plating or pulse reverse plating).

References

[1] A. Brenner, *in* 'Electrodeposition of alloys principles and practice', Vol. 2, Academic Press, New York and London (1963), pp. 413–455.
[2] H. Fukushima, T. Akiyama, S. Agaki and K. Higashi, *Trans. Jpn Inst. Met.* **20** (1979) 358.
[3] M. Cherkaoui, E. Chassaing and K. Vu Quang, *Adv. Mat and Manufacturing Processes* **3**(3) (1988) 407.
[4] M. Degrez and R. Winand, *Oberfläche-Surface* **8** (1990) 8.
[5] E. Chassaing and K. Vu Quang, *Revue de Métallurgie* **88** (1991) 313.
[6] A. L. Pappachan, P. Bagayatkar, A. K. Grover and H. S. Gadiyar, *Trans. Metal Finishers' Ass. India* **1**(1) (1992) 21.
[7] E. J. Podlaha, M. Matlosz and D. Landolt, *J. Electrochem. Soc.* **140**(10) (1993) L149.
[8] E. Chassaing, K. Vu Quang and R. Wiart, *J. Appl. Electrochem.* **19** (1989) 839.
[9] M. Cherkaoui, E. Chassaing and K. Vu Quang, *Plat. & Surf. Finish.* **74**(10) (1987) 50.
[10] C. C. Nee, W. Kim and R. Weil, *J. Electrochem. Soc.* **135**(5) (1988) 1100.
[11] J. Crousier, M. Eyraud, J.-P. Crousier and J. M. Roman, *J. Appl. Electrochem.* **22** (1992) 749.
[12] J. W. Dini, *Metal Finish.* **61**(7) (1963) 52.
[13] R. L. Zeller and U. Landau, *J. Electrochem. Soc.* **138**(4) (1991) 1010.
[14] P. Leisner, G. Bech-Nielsen and P. Moller, *J. Appl. Electrochem.* **23** (1993) 1232.
[15] R. D. Grimm and D. Landolt, *Surf. & Coat. Technol.* **31** (1987) 151.
[16] S. Armyanov and G. Sotirova-Chakarova, *J. Electrochem. Soc.* **139**(12) (1992) 3454.